Autoxidation of the sea ice biomarker proxy IPSO25 in the near-surface oxic layers of Arctic and Antarctic sediments

Jean-Francois Rontani, Lukas Smik, Simon Belt

Autoxidation of the sea ice biomarker proxy $IPSO_{25}$ in the near-surface oxic layers of Arctic and Antarctic sediments

Jean-François Rontani[a*], Lukas Smik[b], Simon T. Belt[b]

[a] *Aix Marseille Univ, Université de Toulon, CNRS/INSU/IRD, Mediterranean Institute of Oceanography (MIO) UM 110, 13288 Marseille, France*

[b] *Biogeochemistry Research Centre, School of Geography, Earth and Environmental Sciences, University of Plymouth, Drake Circus, Plymouth, Devon PL4 8AA, UK*

* Corresponding author. Tel.: +33-4-86-09-06-02; fax: +33-4-91-82-96-41. *E-mail address*: jean-francois.rontani@mio.osupytheas.fr (J.-F. Rontani)

ABSTRACT

Over the last decade or so, the mono- and di-unsaturated highly branched isoprenoid (HBI) lipids IP_{25} (Ice Proxy with 25 carbon atoms) and $IPSO_{25}$ (Ice Proxy for the Southern Ocean with 25 carbon atoms) have emerged as useful proxies for sea ice in the Arctic and Antarctic, respectively. A more complete understanding of their respective proxy signatures, however, requires more detailed knowledge of their stability in the water column and in sediments. In the current study, we focused on the autoxidation of $IPSO_{25}$, first by performing laboratory-based oxidation reactions on a purified sample and characterizing products based on detailed mass spectral analysis. We then analysed for the same oxidation products in near-surface sediments retrieved from the Arctic and the Antarctic, and some suspended organic matter from the Antarctic. Our data show that $IPSO_{25}$ is susceptible to partial autoxidation within the oxic layers of Arctic and Antarctic sediments, while the same processes appear not to be so important in the water column. Although the number of primary autoxidation reactions identified in sediments was not as large as in laboratory experiments, there was evidence for their subsequent modification by biotic degradation. Quantifying the extent of degradation of $IPSO_{25}$ and IP_{25} in sediments, and thus the impact of such process on the use of these biomarkers as paleo sea ice proxies, remains challenging at this stage, since most of the primary oxidation products do not accumulate, likely due to secondary biodegradation reactions. Some interesting differences in reactivity were also observed between $IPSO_{25}$ and IP_{25} present in the same Arctic sediments. This suggests that factors other than environmental control may influence the $IPSO_{25}/IP_{25}$ ratio (i.e. DIP_{25}) in Arctic sediments.

Keywords: $IPSO_{25}$; Degradation; Autoxidation; Arctic and Antarctic sediments; Biotic and abiotic interactions; IP_{25}; DIP_{25}.

1. Introduction

C_{25} and C_{30} highly branched isoprenoid (HBI) alkenes (commonly exhibiting 1–6 double bonds) are ubiquitous biomarkers found in a wide range of marine and lacustrine sediments (Rowland et al., 1990; Belt et al., 2000; Sinninghe Damsté et al., 2004). Despite this, HBIs appear to be biosynthesized by a relatively small number of diatom taxa belonging to the *Haslea, Navicula, Pleurosigma, Berkeleya, Rhizosolenia* and *Pseudosolenia* genera (Volkman et al., 1994; Sinninghe-Damsté et al., 1999; Belt et al., 2001a, 2001b, 2016; Grossi et al., 2004; Brown et al., 2014; Kaiser et al., 2016). Amongst the more recent investigations, a mono-unsaturated C_{25} HBI alkene (3,9,13-trimethyl-6-(1,5-dimethylhexyl)-tetradec-1-ene) was identified in Arctic sea ice and in underlying sediments (Belt et al, 2007; Vare et al, 2009). Since this HBI is believed to only be made by certain Arctic sea ice diatoms (Belt et al., 2007; Brown et al., 2014) and appears relatively stable in the geological record, its analysis in marine sedimentary archives provides a proxy measure of seasonal Arctic sea ice in the past. More commonly referred to as IP_{25} (Ice Proxy with 25 carbon atoms), this HBI has been used as the basis for sea ice reconstructions spanning different Arctic regions and over a range of timescales (see Belt, 2018 for a recent compilation of sea ice reconstructions).

A related di-unsaturated HBI (2,6,10,14-tetramethyl-7-(3-methylpent-4-enyl)-pentadec-6(17)-ene), sometimes referred to as diene II, is co-produced with IP_{25} in the Arctic, and is also biosynthesized by some Antarctic sea ice diatoms (Nichols et al., 1993; Johns et al., 1999; Belt et al., 2016). Interestingly, however, IP_{25} has not been reported in sea ice, sediments or the water column from around the Antarctic. As such, diene II has been proposed as a proxy measure for sea ice in the Southern Ocean, and the term $IPSO_{25}$ (Ice Proxy for the Southern Ocean with 25 carbon atoms) has been recently proposed (Belt et al., 2016). Although $IPSO_{25}$ appears to be a common constituent of Antarctic surface sediments

(for near-coastal regions, at least; Nichols et al., 1993; Johns et al., 1999; Belt et al., 2016; Belt, 2018, 2019), analysis of $IPSO_{25}$ in downcore Antarctic archives has so far resulted in only a relatively small number of palaeo sea ice reconstructions, at least in comparison with IP_{25} for the Arctic (e.g., Collins et al., 2013; Etourneau et al., 2013; Barbara et al., 2016; Campagne et al., 2016; see also Belt, 2018, 2019 for a recent review and summary). Finally, in the Arctic, the ratio $IPSO_{25}/IP_{25}$ (sometimes referred to as DIP_{25}) has previously been proposed as a possible indicator of variability in sea ice conditions or even of sea surface temperatures (SST) (e.g., Fahl and Stein, 2012; Stein et al., 2012; Cabedo-Sanz et al., 2013).

As with all proxies, including those based on individual or combinations of biomarkers, their application requires careful consideration of alteration and preservation between their source and sedimentary environments. It is necessary, therefore, to determine the magnitude and relative importance of various biotic and/or abiotic processes that can influence the preservation of the original source signature. In the case of HBIs, bacterial degradation of some HBIs was studied several decades ago (Robson and Rowland, 1988), yet the effects of photo- and autoxidation on these compounds have been examined only relatively recently.

Motivation for the more recent studies stems partly from the proxy signatures of certain HBIs such as IP_{25} and $IPSO_{25}$, as described above, together with the now well-known high reactivity of terrestrial and marine organic matter, more generally, in the Arctic (Rontani et al., 2012, 2016, 2017). By studying the reactivity of a range of HBI alkenes towards different abiotic processes in solvents and in senescent diatoms (Rontani et al., 2011, 2014), extremely low reactivities of mono- and di-unsaturated HBIs were observed and attributed to the presence of relatively unreactive terminal double bonds. Such lack of reactivity is consistent with the general lack of degradation of IP_{25} in the water column following sea ice melt (Brown et al., 2016; Rontani et al., 2018a). However, lipid autoxidation is not limited to

the water column, and can potentially be an important process in the oxic layers of sediments, especially for regions of low accumulation rates, where near-surface sediments may represent relatively long time intervals (decades to centuries). Indeed, as part of a recent laboratory-based investigation into the autoxidation of IP_{25}, a series of oxidation products were characterized that could also be identified in sediment material from the Canadian Arctic (Rontani et al., 2018a). This study demonstrated the susceptibility of IP_{25} towards autoxidation in Arctic sediments, a process that was more prevalent in cases where sequestered ice algal material experienced relatively long residence times in the oxic layer. On the other hand, the near-ubiquity of IP_{25} in surface sediments from across the Arctic suggests that such oxidation reactions likely perturb its sedimentary content, rather than remove it.

In the present work, we aimed to determine whether $IPSO_{25}$ also undergoes autoxidation in near-surface Arctic and Antarctic sediments and, therefore, whether palaeo sea ice reconstructions using this proxy should consider the possible impact of this type of degradation. To achieve this, oxidation of purified $IPSO_{25}$ was carried out under more powerful oxidative conditions than previously employed (Rontani et al., 2014) and the main products were identified by high resolution mass spectral analysis. The same oxidation products were then analysed for, and quantified, in sediment samples from the Canadian Arctic and the West Antarctic Peninsula (WAP).

2. Experimental

2.1. Sediment sampling

Sediment material from the Arctic was taken from a box core obtained from Barrow Strait (STN 4) in the Canadian Arctic on board the CCGS Amundsen in 2005 (Belt et al.,

2013). The box core was sectioned on board, with sub-samples (1 cm resolution) then frozen (–20 ℃) prior to being freeze-dried and stored (–20 ℃ to +4 °C) prior to analysis (Rontani et al., 2018a). The redox boundary layer was identified using the change (reduction) in Mn content as described previously (Vare et al., 2009; Brown, 2011 and References cited therein). Sediment material from the WAP (see Belt et al., 2016 for details of locations) was obtained from the upper 0–1 cm of box cores collected between 2002 and 2011 and then held at the British Antarctic Survey (UK) or the British Ocean Sediment Core Research Facility (BOSCORF, UK) at +4 °C. Suspended particulate matter (SPM) were obtained off the coast of East Antarctica as described previously (Rontani et al., 2018b) (Supplementary Fig. S1).

2.2. Chemicals

A sample of purified $IPSO_{25}$ was obtained from a culture of the marine diatom *Haslea ostrearia* as described previously (Johns et al., 1999).

Treatment of $IPSO_{25}$ with a stoichiometric amount of perchloroperbenzoic acid in dry dichloromethane (4 h at 50 °C) mainly afforded 1,2-epoxy-2-(4-methylpentyl)-3-(3-methylpent-4-enyl)-6,10-dimethylundecane (**1**) (93%) (Belt et al., 2007) and to a lower extent 1,2-epoxy-3,9,13-trimethyl-6-(1-methylidene-5-methylhexyl)-tetradecane (**2**) (7%) (total yield 85%). Differentiation between these two isomers was difficult due to their very similar mass spectra and so required $LiAlH_4$-reduction to the corresponding alcohols (see below).

Oxidation of $IPSO_{25}$ using $RuCl_3$ and *tert*-butyl hydroperoxide in cyclohexane at room temperature for 16 h (Seki et al., 2008) and subsequent $NaBH_4$-reduction in ether-methanol (4:1, v/v) produced 6-methylidene-2,10,14-trimethyl-7-(3-methylpent-4-enyl)-pentadecan-5-ol (**3**) and 3,9,13-trimethyl-6-(1-methylidene-5-methylhexyl)-tetradec-1-en-3-ol (**4**) in low yield. It is interesting to note that using a mixture of $RuCl_3$ and *tert*-butyl hydroperoxide failed to attack the tertiary allylic position at C-7, likely due to steric hindrance.

147 $LiAlH_4$-reduction of the mixture of epoxides **1** and **2** in dry diethyl ether (1 h at room
148 temperature) afforded 2,6,10,14-tetramethyl-7-(3-methylpent-4-enyl)-pentadecan-6-ol (**5**) and
149 3,9,13-trimethyl-6-(1-methylidene-5-methylhexyl)-tetradecan-2-ol (**6**), respectively (total
150 yield 95%).
151 Treatment of $IPSO_{25}$ with a stoichiometric amount of OsO_4 in dioxane-pyridine (8:1,
152 v/v) at room temperature for 1 h (McCloskey and McClelland, 1965) afforded 2-(4-
153 methylpentyl)-3-(3-methylpent-4-enyl)-6,10-dimethylundecane-1,2-diol (**7**) (yield 60%).
154 3,9,13-Trimethyl-6-(1-methylene-5-methylhexyl)-tetradecane-1,2-diol (**8**) was
155 obtained in small amounts after hydrolysis of the epoxide **2** in a mixture of MeOH and HCl
156 2N (5:1, v/v) at 50 °C for 2 h. Under these conditions epoxide **1** mainly isomerized to allylic
157 alcohols.
158 3,7,11,15-Tetramethylhexadecan-1,2-diol (**9**) was produced by $Pd/CaCO_3$-catalysed
159 hydrogenation of 3-methylidene-7,11,15-trimethylhexadecan-1,2-diol (**10**) (Rontani et al.,
160 2018), whose synthesis from phytol was described previously (Rontani and Aubert, 2005).
161 2,6,10,14-Tetramethylpentadecan-2-ol (**11**) was produced by condensation of 6,10,14-
162 trimethylpentadecan-2-one (**12**) with methyllithium in anhydrous diethyl ether as previously
163 described (Rontani et al., 2013a).
164
165 *2.3. Induction of autoxidation in solvent*
166 Autoxidation experiments were performed under an atmosphere of air in 15 ml screw-
167 cap flasks containing $IPSO_{25}$ (10 µg), *tert*-butyl hydroperoxide (300 µl of a 6.0 M solution in
168 decane), di-*tert*-butyl nitroxide (1.2 mg) and hexane (2 ml). After stirring, the flask was
169 incubated in the dark at 65 °C. A relatively high temperature was selected in order to
170 accelerate the autoxidation reactions. Aliquots (200 µl) were withdrawn from the reaction
171 mixture after incubation for different times. Each sub-sample was evaporated to dryness under

a stream of nitrogen and analyzed by gas chromatography–electron ionization quadrupole time of flight mass spectrometry (GC–QTOF) after $NaBH_4$ reduction (Section 2.5) and derivatization (Section 2.7) for identification of hydroxylated oxidation products.

2.4. Reduction of oxidation products

Hydroperoxides resulting from $IPSO_{25}$ oxidation were reduced to the corresponding alcohols by reaction with excess $NaBH_4$ in diethyl ether:methanol (4:1, v/v) at room temperature (1 h). After reduction, a saturated solution of NH_4Cl (10 ml) was added cautiously to remove any unreacted reducing agent; the pH was adjusted to 1 with dilute HCl (2 N) and the mixture shaken and extracted with hexane:chloroform (5 ml, 4:1, v/v; ×3). The combined extracts were dried over anhydrous Na_2SO_4, filtered and evaporated to dryness under a stream of nitrogen.

2.5. Sediment and SPM treatment

Sediments or SPM material (collected on GF/F filters, porosity 0.8 µm) were placed in MeOH (15 ml) and hydroperoxides were reduced to the corresponding alcohols with excess $NaBH_4$ (70 mg, 30 min at 20 °C). Following the reduction step, water (15 ml) and KOH (1.7 g) were added and the mixture saponified by refluxing (2 h). After cooling, the contents of the flask were acidified (HCl, to pH 1) and extracted three times with dichloromethane (DCM) (30 ml). The combined DCM extracts were dried over anhydrous Na_2SO_4, filtered and concentrated to give the total lipid extract (TLE). Since $IPSO_{25}$ oxidation product content was quite low relative to other lipids, accurate quantification required further separation of the TLE using column chromatography (silica; Kieselgel 60, 8 × 0.5 cm). $IPSO_{25}$ was recovered in the hexane eluate and its oxidation products in the dichloromethane eluate.

2.6. Derivatization

In order to analyse for hydroxylated products (i.e. alcohols and carboxylic acids), lipid extracts were derivatized by dissolving them in 300 µl pyridine/*bis*-(trimethylsilyl)trifluoroacetamide (BSTFA; Supelco; 2:1, v/v) and silylated (50 °C, 1 h). After evaporation to dryness under a stream of N_2, the derivatized residue was re-dissolved in 100 µl BSTFA (to avoid desilylation of fatty acids), together with an amount of solvent (ethyl acetate) dependent on the mass of the extract, and then analyzed using GC–QTOF and GC–MS/MS.

2.7. GC–QTOF analyses

Accurate mass spectra were obtained with an Agilent 7890B/7200 GC–QTOF System (Agilent Technologies, Parc Technopolis - ZA Courtaboeuf, Les Ulis, France). A cross-linked 5% phenyl-methylpolysiloxane (Macherey Nagel; Optima 5-MS Accent) column (30 m × 0.25 mm, 0.25 µm film thickness) was employed. Analysis was performed with an injector operating in pulsed splitless at 280 °C and the oven temperature programmed from 70 °C to 130 °C at 20 °C/min, then to 250 °C at 5 °C/min and then to 300 °C at 3 °C/min. The carrier gas (He) was maintained at 0.69×10^5 Pa until the end of the temperature program. Instrument temperatures were 300 °C for the transfer line and 230 °C for the ion source. Accurate mass spectra were recorded across the range *m*/*z* 50–700 at 4 GHz with nitrogen as collision gas (1.5 ml/min). The QTOF-MS instrument provided a typical resolution ranging from 8009 to 12252 from *m*/*z* 68.9955 to 501.9706. Perfluorotributylamine (PFTBA) was utilized for daily MS calibration. Structural assignments were based on interpretation of accurate mass spectral fragmentations and confirmed by comparison of retention times and mass spectra of oxidation products with those of authentic synthesized compounds.

222 *2.8. GC–MS/MS analyses*

223 GC–EIMS/MS experiments were performed using an Agilent 7890A/7010 tandem
224 quadrupole gas chromatograph system equipped with a HES source (Agilent Technologies,
225 Parc Technopolis - ZA Courtaboeuf, Les Ulis, France). A cross-linked 5% phenyl-
226 methylpolysiloxane (Agilent; HP-5MS) (30 m × 0.25 mm, 0.25 μm film thickness) capillary
227 column was employed. Analyses were performed with an injector operating in pulsed splitless
228 mode set at 270 °C and the oven temperature programmed from 70 °C to 130 °C at 20
229 °C/min, then to 250 °C at 5 °C/min and then to 300 °C at 3 °C/min. The pressure of the carrier
230 gas (He) was maintained at 0.69×10^5 Pa until the end of the temperature program and then
231 programmed from 0.69×10^5 Pa to 1.49×10^5 Pa at 0.04×10^5 Pa/min. The following mass
232 spectrometric conditions were employed: electron energy, 70 eV; transfer line, 300 °C; source
233 temperature, 230 °C; quadrupole 1 temperature, 150 °C; quadrupole 2 temperature, 150 °C;
234 collision gas (N_2) flow, 1.5 ml/min; quench gas (He) flow, 2.25 ml /min; mass range, 50–700
235 Da; cycle time, 313 ms. Collision induced dissociation (CID) was optimized by using
236 collision energies at 5, 10, 15 and 20 eV.

237 Quantification of oxidation products **3**, **5** and **7** was carried out with external standards
238 in multiple reaction monitoring (MRM) mode. Precursor ions were selected from the more
239 intense and specific ions observed in EI mass spectra. Due to the very low amounts of $IPSO_{25}$
240 available, these compounds could not be produced in sufficient amounts to be used as external
241 standard during their quantification in sediment samples. TMS derivative of structurally
242 similar isoprenoid compounds (3-methylidene-7,11,15-trimethylhexadecan-1,2-diol (**10**) for
243 compound **3**, 2,6,10,14-tetramethylpentadecan-2-ol (**11**) for compound **5** and 3,7,11,15-
244 tetramethylhexadecan-1,2-diol (**9**) for compound **7**) (see Appendix) were thus used as external
245 standards. Correction factors that took into account the proportion of the selected precursor

246 ion in the EIMS of each compound and that of the selected MRM transition in each CID-MS
247 were employed.
248
249 **3. Results**
250
251 *3.1. Autoxidation of $IPSO_{25}$ in solvent*
252 A number of different oxidation products could be detected after incubation of $IPSO_{25}$
253 in hexane in the presence of *tert*-butyl hydroperoxide (radical enhancer) and di-*tert*-butyl
254 nitroxide (radical initiator) (Porter et al., 1995) at 65 °C and subsequent $NaBH_4$-reduction and
255 silylation. Comparison of retention times and accurate mass spectra of these compounds
256 (Figs. 1 and 2) with qualitative standards prepared by oxidation of purified $IPSO_{25}$ (Section
257 2.2) allowed formal identification of compounds **1** (59.2%), **2** (5.9%), **3** (9.3%), **4** (10.2%)
258 and **7** (traces). A compound derived from the attack of the terminal tertiary carbon atoms was
259 also detected and tentatively attributed to 10-methylidene-2,6,14-trimethyl-9-(3-methylpent-
260 4-enyl)-pentadecan-2-ol (**13**) or 6-methylidene-2,10,14-trimethyl-7-(3-methylpent-4-enyl)-
261 pentadecan-2-ol (**14**) (7.6%) on the basis of the accurate mass fragmentations observed (Fig.
262 1D).
263
264 *3.2. Autoxidation of $IPSO_{25}$ in Arctic and Antarctic sediments*
265 The DCM eluates obtained after chromatographic fractionation of the total lipid
266 extracts from the sediments investigated were analysed in MRM mode. The use of the
267 transitions *m*/*z* 365 → 275, *m*/*z* 365 → 135 and *m*/*z* 365 → 149 and the comparison of
268 retention time with the oxidation products characterized during the thermal incubation
269 reactions allowed the unambiguous detection of the alcohol **3** (Fig. 3). In contrast, we failed to
270 detect the oxidation products **1**, **2** and **4**. Taking into account: (i) the presence of the $IPSO_{25}$

oxidation product **3** in the sediments and (ii) the well-known lability of epoxides, we searched for the presence of the reduction and hydrolysis products of the main oxidation product **1** (i.e. 2,6,10,14-tetramethyl-7-(3-methylpent-4-enyl)-pentadecan-6-ol (**5**) (Fig. 2A) and 2-(4-methylpentyl)-3-(3-methylpent-4-enyl)-6,10-dimethylundecane-1,2-diol (**7**) (Fig. 2C)). By using appropriate MRM transitions, we were able to detect the tertiary alcohol **5** in DCM eluates of both Arctic and Antarctic sediments (Fig. 4). In contrast, diol **7** could only be identified in the Arctic sediment extracts (Fig. 5).

As described in Section 2.8, quantification of compounds **3**, **5** and **7** involved the use of TMS derivatives of structurally similar isoprenoid compounds as external standards. The transitions employed for quantification were (i) *m*/*z* 365 → 275 and *m*/*z* 353 → 263 (loss of trimethylsilanol by the precursor ion) for the alcohol **3** and the standard **10**, respectively; (ii) *m*/*z* 353 → 117 and *m*/*z* 341 → 117 (formation of the product ion TMS-O^+=CH–CH_3) for the tertiary alcohol **5** and the standard **11**, respectively; (iii) *m*/*z* 423 → 333 and *m*/*z* 355 → 265 (loss of trimethylsilanol by the precursor ion) for the diol **7** and the standard **9**, respectively. As indicated in Section 2.8, corrective factors were applied to accommodate structural differences between the oxidation product and the corresponding standard. The resulting concentrations of compounds **3**, **5** and **7** are given in Tables 1 and 2.

3.3. Autoxidation of $IPSO_{25}$ in Antarctic SPM

We also analysed for $IPSO_{25}$ oxidation products in lipid extracts of suspended particles collected at different water depths in the polynya region west of the Dalton Iceberg Tongue (East Antarctica) and where an intense autoxidation of some other lipids was previously observed (Rontani et al., 2018b). However, compounds **3**, **5** and **7** could not be identified in any of the samples analysed.

4. Discussion

4.1. Autoxidation of $IPSO_{25}$ in solvent

It is well-known that addition of ROO• radicals to a C=C bond competes with allylic hydrogen abstraction when there is a double bond that is either conjugated or 1,1-disubstituted (Schaich, 2005). Consistent with this, we observed efficient addition of peroxyl radicals to the 1,1-disubstituted 6-17 double bond of $IPSO_{25}$ affording epoxide **1** as the major product (59.2% of total oxidation products) after fast intramolecular homolytic substitution (Fossey et al., 1995) (Fig. 6). In contrast, addition to the terminal 23-24 double bond was relatively minor (5.9% of total oxidation products). Addition of peroxyl radicals to the 6-17 double bond also resulted in the formation of trace amounts of the diol **7** after subsequent oxygen addition and hydrogen abstraction (Fig. 6).

Parallel to these peroxyl radical addition reactions was a series of competitive hydrogen abstraction reactions leading to the formation of hydroperoxides **15-18** (see Appendix), which manifest as alcohols **3**, **4**, **13** and **14** following $NaBH_4$-reduction during treatment. Hydrogen atom abstraction from the allylic carbon atoms 5 and 22 of $IPSO_{25}$ and subsequent oxidation of the resulting radicals to yield hydroperoxides **15** and **16**, respectively (Fig. 6), is as expected given the relatively stable allylic radicals formed (Fig. 6), with the additional formation of hydroperoxides **17** and **18** presumably attributable to the stability of their respective tertiary radical precursors. Surprisingly, we failed to detect oxidation products resulting from hydrogen atom abstraction at carbon 7, despite the stability of the tertiary allylic radical formed. These results are consistent with the very low efficiency of autoxidative processes at the allylic C-7 previously observed in the case of (6-17, 9-10, 23-24) HBI triene (Rontani et al., 2014). We suggest that the lack of reaction at C-7 results from steric hindrance during hydrogen abstraction by the bulky *tert*-butylperoxyl radicals employed

during the incubation and is supported by the lack of oxidation of the allylic carbon 7 observed during treatment of $IPSO_{25}$ with $RuCl_3$- *tert*-butyl hydroperoxide (see Section 2.2). Hydrogen atom abstraction from non-allylic tertiary carbon atoms appeared to be limited to the external tertiary carbon atoms 2 and 14 of the molecule (and not to carbon 10), also likely due to steric hindrance.

4.2. Degradation of $IPSO_{25}$ in Arctic and Antarctic sediments

Despite the relative recalcitrance of mono- and di-unsaturated HBIs towards free radical oxidation, reported previously (Rontani et al., 2011, 2014), oxidation product **3** could be detected in most of the Arctic and Antarctic sediments (Tables 1 and 2), confirming the partial autoxidation of $IPSO_{25}$ in both regions. On the other hand, the failure to detect the major oxidation product of this diene in the incubation experiments (i.e. compound **1**) likely results from: (i) the lack of specificity of its main MRM transitions, thus making it difficult to identify, (ii) an intense degradation during the treatment ($NaBH_4$-reduction, alkaline hydrolysis and acidification) or (iii) the well-known biotic and abiotic lability of epoxides in sediments, more generally. Indeed, epoxides may undergo alcoholysis and hydrolysis during alkaline hydrolysis and are converted to chlorohydrins during acidification with HCl (Marchand and Rontani, 2001).

Some epoxides are also slowly reduced to alcohols during $NaBH_4$-reduction (Zabeti et al., 2010), but this is not the case for epoxide **1**. From a biological perspective, these epoxides react readily with a large number of cell components such as DNA or proteins (Swaving and de Bont, 1998) so their removal is essential for bacteria to survive. This involves two main types of enzymes: glutathione transferases (GSTs) (which catalyse the reduction of the epoxide ring to an alcohol, Kieslich et al., 1986) and epoxide hydrolases (which catalyse the hydrolysis of the epoxide ring to a diol, Michaels et al., 1980; Rustemov et al., 1991).

Moreover, epoxides may also be hydrolysed abiotically (Minerath et al., 2009) and rearranged to carbonyl compounds in sediments with high clay content (Ruiz-Hitzky and Casal, 1985).

The presence of the tertiary alcohol **5** in the sediments investigated (Tables 1 and 2), may therefore potentially be attributed to the reduction of the epoxide ring of the $IPSO_{25}$ oxidation product **1** by sedimentary bacteria (Fig. 7). However, alcohol **5** might also be produced directly from $IPSO_{25}$ by bacteria after hydration (pathway II in Fig. 7) or epoxidation (pathway III in Fig. 7) and subsequent reduction (pathway IV in Fig. 7). Indeed, the involvement of hydration during anaerobic bacterial degradation of isoprenoid alkenes (squalene, pristenes and phytenes, Rontani et al., 2002, 2013a) and *n*-alk-1-enes (Grossi et al., 2011) was demonstrated previously. On the other hand, bacterial epoxidation (mediated by cytochrome P-450-dependent monooxygenases) can produce epoxides from a broad range of lipophilic substrates such as *n*-alkenes (Soltani et al., 2004), terpenes (Duetz et al., 2003), unsaturated fatty acids (for a review see Ratledge, 1994) and alkenones (Zabeti et al., 2010). Since bacterial epoxidation should act more intensively on the terminal 23-24 double bond due to the better proximity of the terminal double bond to the heme iron of cytochrome P-450 (Andersen et al., 1997), the formation of epoxide **2** (Fig. 7) and its degradation products would thus be expected. However, the absence of alcohol **6** (resulting from the reduction of epoxide **2** or hydration of the 23-24 double bond of $IPSO_{25}$ (Fig. 7)) in the sediments analyzed points to the lack of such bacterial processes, so the formation of alcohol **5** seems thus to mainly result from bacterial reduction of the epoxide ring of autoxidation product **1**.

Further, due to the probable low reactivity of monooxygenases towards the 6-17 double bond of $IPSO_{25}$, the formation of diol **7** may be attributed to the biotic (induced by epoxide hydrolases) or abiotic (clay-catalyzed) hydrolysis of epoxide **1** (pathways V and VI in Fig. 7). The lack of methoxyhydrins and chlorohydrins derived from the degradation of the epoxide **1** in the presence of methanol and hydrochloric acid, respectively, also allow us to

371 exclude the possible production of diol **7** during sample treatment (alkaline hydrolysis and
372 acidification).

373 Surprisingly, diol **8** could not be detected during MRM analyses of the sediment
374 extracts, despite the previous detection of its close structural analog (i.e. diol **19**) as an
375 oxidation product of IP_{25} in the same (STN 4) sediments (Rontani et al., 2018a). We attribute
376 this to (i) the possible coelution of diols **7** and **8** and (ii) the very weak abundance of the
377 precursor ion at *m*/*z* 423 in the mass spectrum of its TMS derivative (Fig. 2D), rather than
378 from a lack of microbial degradation of $IPSO_{25}$.

379 In the sediments from the Arctic (STN 4), we also note the generally increasing
380 proportion of $IPSO_{25}$ oxidation products with depth below the redox boundary (Fig. 8),
381 indicative of a progressive reduction of hydroperoxide **15** (produced in the oxic layer) to the
382 corresponding alcohol **3**, together with reduction and hydrolysis of the epoxide **1** to yield
383 alcohol **5** and diol **7**. However, due to the proposed action of sedimentary bacteria on the
384 autoxidation products of $IPSO_{25}$ (see earlier), the very low amounts of compounds **3**, **5** and **7**
385 relative to their parent compound (< 1%; Fig. 8) likely underestimate the extent of abiotic
386 degradation of $IPSO_{25}$, more generally.

387 In the Antarctic surface sediments, the proportion of oxidation products was always
388 low, ranging from 0.02 to 1.1% of the residual $IPSO_{25}$ (Table 1). These differences may
389 potentially be attributed to: (i) the ability for sedimentary bacterial communities to degrade
390 the primary $IPSO_{25}$ autoxidation products, as described above, or (ii) the different residence
391 times of algal material within the oxic layer of sediments, which may vary considerably
392 according to location. On the other hand, the variable degradation extent may reflect the
393 different times that the sediments have been kept in storage following collection; however, for
394 the samples analyzed, the lowest percentages of degradation products were observed in the
395 oldest samples (i.e. in BC 313/316 collected in 2002 compared to the other box cores

collected in 2008 and 2011; Table 1). These results, and those obtained previously for IP_{25} (Rontani et al., 2018a), highlight the importance of the measurement of redox boundary layers in upper sections of sediment cores and sedimentation rates to estimate the residence time of algal material in the oxic environment and thus the extent of autoxidative degradation and its impact on paleo sea ice reconstruction based on the use of HBI tracers.

4.3. Degradation of $IPSO_{25}$ in Antarctic SPM

The failure to detect compounds **3**, **5** and **7** in lipid extracts of strongly autoxidized suspended particles (Rontani et al., 2018b) collected at different water depths in the polynya region west of the Dalton Iceberg Tongue (East Antarctica) is in good agreement with: (i) the relative recalcitrance of di-unsaturated HBIs towards free radical oxidation processes (Rontani et al., 2011, 2014), and (ii) the expected short residence time of highly aggregated ice algae (i.e. the source of $IPSO_{25}$) (Riebesell, 1991; Alldredge et al., 1993; Passow, 2002) within the water column. It also enables us to exclude the possible biological formation of these compounds in ice algae.

4.4. Potential effects of degradation processes on the DIP_{25} index

Due to the co-occurrence of $IPSO_{25}$ (generally reported as diene II in the Arctic) and IP_{25} in Arctic sea ice, particles and sediments under sea ice (Belt et al., 2007; Vare et al., 2009), it has been suggested that the ratio between these two biomarkers (viz $IPSO_{25}/IP_{25}$ or DIP_{25} (Cabedo-Sanz et al., 2013)) may potentially provide further insights into Arctic sea ice conditions (e.g., Fahl and Stein, 2012; Stein et al., 2012; Cabedo-Sanz et al., 2013). It has also been suggested that variable DIP_{25} might be indicative of changes to SST based on some empirical observations and alignment with other SST proxies (Vare et al., 2009; Cabedo-Sanz et al., 2013; Xiao et al., 2013; Müller and Stein, 2014; Ruan et al., 2017); however, there are

421 as yet no in situ data to support these interpretations (Belt, 2018). In general, proxies based on
422 ratios of biomarkers are better at accommodating the effects of degradative processes, even if
423 such effects cannot be totally eliminated. Indeed, it was previously demonstrated that, under
424 some conditions, autoxidative and biodegradation processes may act selectively on $C_{37:2}$ and
425 $C_{37:3}$ alkenones, thus negatively impacting on the $U^{K'}_{37}$ index (for a review, see Rontani et al.,
426 2013b). It is feasible, therefore, that differential degradation of IP_{25} and $IPSO_{25}$ may also
427 influence the DIP_{25} ratio, with substantially increased values, as seen in some sedimentary
428 records (Fahl and Stein, 2012; Müller and Stein, 2014) resulting from a preferential
429 degradation of IP_{25}. Previously, however, autoxidative degradation of these two HBIs
430 measured in solvents (Rontani et al., 2014), showed a higher degradation rate for $IPSO_{25}$ (k =
431 0.004 h^{-1}) compared to IP_{25} (k = 0.001 h^{-1}). Unfortunately, due to the mineralisation of the
432 major part of substrates by bacteria, comparison of the efficiency of bacterial degradation
433 processes on IP_{25} and $IPSO_{25}$ on the basis of the quantities of metabolites detected is difficult.
434 However, we note that significant proportions (up to 35% of the residual substrate) of 2,8,12-
435 trimethyl-5-(1,5-dimethylhexyl)-tridecanoic acid (**20**), resulting from bacterial cleavage of the
436 23-24 double bond of IP_{25}, were detected in sediments from Barrow Strait (i.e. STN 4)
437 (Rontani et al., 2018c), while we failed to detect the corresponding metabolite of $IPSO_{25}$ (i.e.
438 2,8,12-trimethyl-5-(1-methylidene-5-methylhexyl)-tridecanoic acid (**21**)) in the same
439 sediments. This suggests a preferential bacterial degradation of IP_{25}, which could potentially
440 be attributed to the presence of toxic autoxidative epoxides in algal material containing
441 $IPSO_{25}$, which are in lower abundance (or absent) in the case of IP_{25}. More detailed analyses
442 of factors that control the DIP_{25} ratio, however, will be required in the future.
443
444 *4.5. Consequences for IP_{25}, $IPSO_{25}$ and DIP_{25}-based sea ice reconstructions*

As with all lipid-based proxies, those involving HBIs such as IP_{25} and $IPSO_{25}$ require careful consideration of their alteration and preservation during transport through the water column and deposition in sediments, including determining the magnitude and relative importance of biotic and/or abiotic processes. While both autoxidative and bacterial degradation products of IP_{25} were identified and quantified previously in Arctic surficial sediments (Rontani et al., 2018c), here we demonstrated that $IPSO_{25}$ may also be affected by such processes in Arctic and Antarctic sediments. At this stage, the characterisation of signature degradation products from these biotic and abiotic processes mainly provides useful 'qualitative' indicators of diagenetic alteration of these two paleo sea ice tracers. Unfortunately, subsequent reaction of most of the primary oxidation products by sedimentary bacteria limits their accumulation in sediments, thereby preventing any accurate quantitative estimates of the extent of degradation of IP_{25} and $IPSO_{25}$, and thus of the ratio between them (i.e. DIP_{25}). The impacts of sedimentary degradation of IP_{25} and $IPSO_{25}$ on their use as paleo sea ice proxies therefore remains difficult to assess at this stage. On the other hand, the somewhat higher accumulation of 2,8,12-trimethyl-5-(1,5-dimethylhexyl)-tridecanoic acid (**20**) in some oxic sediments could potentially provide semi-quantitative estimates of the role of bacterial degradation of IP_{25} (Rontani et al., 2018c).

5. Conclusions

The detection of reduced or hydrolyzed autoxidation products of $IPSO_{25}$ in Arctic and Antarctic sediments demonstrated that this proxy may be partially degraded abiotically in near-surface oxic sediments, especially in the case of sediment cores containing relatively thick oxic layers representing long times of deposition. Unfortunately, due to its high biotic and abiotic lability, the major autoxidation product formed (epoxide **1**) does not accumulate in

sediments. In contrast, $IPSO_{25}$ appeared to be essentially unaffected by autoxidation processes in the water column.

The results obtained during this work also confirmed that, in the environment, biotic and abiotic degradation processes cannot be considered separately. Indeed, their interactions, although complex, need to be taken into account in any organic geochemical assessment.

Autoxidation reactions of HBIs appear to occur primarily at the unsaturated or allylic carbon atoms within the lipid framework. However, the production of compounds such as **13** or **14** observed during $IPSO_{25}$ autoxidation, and the previous detection of degradation products of IP_{25} in Arctic sediments resulting from the free radical oxidation of its saturated tertiary carbon atoms (Rontani et al., 2018a), clearly show that autoxidation processes can also affect saturated compounds when algal or bacterial material experiences long residence times in the oxic layer of sediments.

Acknowledgements

Financial support from the Centre National de la Recherche Scientifique (CNRS) and the Aix-Marseille University is gratefully acknowledged. Thanks are due to the FEDER OCEANOMED (N° 1166-39417) for the funding of the apparatus employed. LS and STB are grateful to the University of Plymouth for financial support. We thank Leanne Armand and Amy Leventer for providing the SPM samples. Thanks are due to two anonymous reviewers and to the Associate Editor for their useful and constructive comments.

Associate Editor–**Stuart Wakeham**

References

Alldredge, A.L., Passow, U., Logan, B.E., 1993. The abundance and significance of a class of large, transparent organic particles in the ocean. Deep-Sea Research Part I–Oceanographic Research Papers 40, 1131–1140.

Andersen, J.F., Walding, J.K., Evans, P.H., Bowers, W.S., Feyereisen, R., 1997. Substrate specificity for the epoxidation of terpenoids and active site topology of house fly cytochrome P450 6A1. Chemical Research in Toxicology 10, 156–164.

Barbara, L., Crosta, X., Leventer, A., Schmidt, S., Etourneau, J., Domack, E., Massé, G., 2016. Environmental responses of the Northeast Antarctic Peninsula to the Holocene climate variability. Paleoceanography, 31, 131–147.

Belt, S.T., Allard, W.G., Massé, G., Robert, J.-M., Rowland, S.J., 2000. Highly branched isoprenoids (HBIs): identification of the most common and abundant sedimentary isomers. Geochimica et Cosmochimica Acta 64, 3839–3851.

Belt, S.T., Massé, G., Allard, W.G., Robert, J.-M., Rowland, S.J., 2001a. Identification of a C_{25} highly branched isoprenoid triene in the freshwater diatom *Navicula sclesvicensis*. Organic Geochemistry 32, 1169–1172.

Belt, S.T., Massé, G., Allard, W.G., Robert, J.-M., Rowland, S.J., 2001b. C_{25} highly branched isoprenoid alkenes in planktonic diatoms of the *Pleurosigma* genus. Organic Geochemistry 32, 1271–1275.

Belt, S.T., Massé, G., Rowland, S.J., Poulin, M., Michel, C., LeBlanc, B., 2007. A novel chemical fossil of palaeo sea ice: IP_{25}. Organic Geochemistry 38, 16–27.

Belt, S.T., Smik, L., Brown, T.A., Kim, J.H., Rowland, S.J., Allen, C.S., Gal, J.K., Shin, K.H., Lee, J.I., Taylor, K.W.R., 2016. Source identification and distribution reveals the potential of the geochemical Antarctic sea ice proxy $IPSO_{25}$. Nature Communications 7, 12655.

519 Belt, S.T., 2018. Source-specific biomarkers as proxies for Arctic and Antarctic sea ice.
520 Organic Geochemistry 125, 277–298.
521 Belt, S.T., 2019. What do IP_{25} and related biomarkers really reveal about sea ice change?
522 Quaternary Science Reviews 204, 216–219.
523 Brown, T.A., 2011. Production and preservation of the Arctic sea ice diatom biomarker IP_{25}.
524 PhD thesis, University of Plymouth, UK.
525 Brown, T.A., Belt, S.T., Cabedo-Sanz, P., 2014. Identification of a novel diunsaturated C_{25}
526 highly branched isoprenoid in the marine tube-dwelling diatom *Berkeleya rutilans*.
527 Environmental Chemistry Letters 12, 455–460.
528 Cabedo-Sanz, P., Belt, S.T., Knies, J., Husum, K., 2013. Identification of contrasting seasonal
529 sea ice conditions during the Younger Dryas. Quaternary Science Reviews 79, 74–86.
530 Campagne, P., Crosta, X., Schmidt, S., Houssais, M.N., Ther, O., Massé, G., 2016.
531 Sedimentary response to sea ice and atmospheric variability over the instrumental
532 period off Adélie Land, East Antarctica. Biogeosciences 13, 4205–4218.
533 Collins, L.G., Allen, C.S., Pike, J., Hodgson, D.A., Weckström, K., Massé, G., 2013.
534 Evaluating highly branched isoprenoids (HBIs) as an Antarctic sea-ice proxy in deep-
535 water glacial sediments. Quaternary Science Reviews 79, 87–98.
536 Duez, W.A., Bouwmeester, H., Beilen, J.B., Witholt, B., 2003. Biotransformation of limonene
537 by bacteria, fungi, yeasts and plants. Applied Microbiology and Biotechnology 61,
538 299–301.
539 Etourneau, J., Collins, L.G., Willmott, V., Kim, J.H., Barbara, L., Leventer, A., Schouten, S.,
540 Sinninghe Damsté, J.S., Bianchini, A., Klein, V., Crosta, X., Massé, G., 2013.
541 Holocene climate variations in the western Antarctic Peninsula: evidence for sea ice
542 extent predominantly controlled by changes in insolation and ENSO variability.
543 Climate of the Past 9, 1431–1446.

544 Fahl, K., Stein, R., 2012. Modern seasonal variability and deglacial/Holocene change of
545 central Arctic Ocean sea-ice cover: New insights from biomarker proxy records. Earth
546 and Planetary Science Letters 351–352, 123–133.
547 Fossey, J., Lefort, D., Sorba, J., 1995. Free Radicals in Organic Chemistry. Masson, Paris.
548 Grossi, V., Beker, B., Geenevasen, J.A.J., Schouten, S., Raphel, D., Fontaine, M.-F.,
549 Sinninghe Damsté, J.S., 2004. C_{25} highly branched isoprenoid alkenes from the marine
550 benthic diatom *Pleurosigma strigosum*. Phytochemistry 65, 3049–3055.
551 Grossi, V., Cravo-Lauro, C., Rontani, J.-F., Cros, M., Hirschler-Réa, A., 2011. Anaerobic
552 oxidation of *n*-alkenes by sulphate-reducing bacteria from the genus *Desulfatiferula*:
553 *n*-ketones as potential metabolites. Research in Microbiology 162, 915–922.
554 Johns, L., Wraige, E.J., Belt, S.T., Lewis, C.A., Massé, G., Robert, J.M., Rowland, S.J., 1999.
555 Identification of a C_{25} highly branched isoprenoid (HBI) diene in Antarctic sediments,
556 Antarctic sea-ice diatoms and cultured diatoms. Organic Geochemistry 30, 1471–
557 1475.
558 Kaiser, J., Belt, S.T., Tomczak, T., Brown, T.A., Wasmund, N., Arz, H.W., 2016. C_{25} highly
559 branched isoprenoid alkenes in the Baltic Sea produced by the marine planktonic
560 diatom *Pseudosolenia calcar-avis*. Organic Geochemistry 93, 51–58.
561 Kieslich, K. Abraham, W.R., Stumpf, B., Thede, B., Washausen, P., 1986. Transformation of
562 terpenoids. In: Brunke, E.J. (Ed.), Progress in Essential Oil Research. Walter de
563 Gruyter & Co., Berlin, pp. 368–394.
564 McCloskey, J.A., McClelland, M.J., 1965. Mass spectra of O-isopropylidene derivatives of
565 unsaturated fatty esters, Journal of the American Chemical Society 87, 5090–5093.
566 Marchand, D., Rontani, J.-F., 2001. Characterisation of photooxidation and autoxidation
567 products of phytoplanktonic monounsaturated fatty acids in marine particulate matter
568 and recent sediments. Organic Geochemistry 32, 287–304.

569 Michaels, B.C., Ruettinger, R.T., Fulco, A.J., 1980. Hydration of 9,10-epoxypalmitic acid by
570 a soluble enzyme from *Bacillus megaterium*. Biochemical and Biophysical Research
571 Communications 92, 1189–1195.
572 Minerath, E.C., Schultz, M.P., Elrod, M.J., 2009. Kinetics of the reactions of isoprene-derived
573 epoxides in model tropospheric aerosol solutions. Environmental Science Technology
574 43, 8133–8139.
575 Müller, J., Stein, R., 2014. High-resolution record of late glacial sea ice changes in Fram
576 Strait corroborates ice-ocean interactions during abrupt climate shifts. Earth and
577 Planetary Science Letters 403, 446–455.
578 Nichols, D.S., Nichols, P.D., Sullivan, C.W., 1993. Fatty acid, sterol and hydrocarbon
579 composition of Antarctic sea ice diatom communities during the spring bloom in
580 McMurdo Sound. Antarctic Science 5, 271–278.
581 Passow, U., 2002. Transparent exopolymer particles (TEP) in aquatic environments. Progress
582 in Oceanography 55, 287–333.
583 Porter, N.A., Caldwell, S.E., Mills, K.A., 1995. Mechanisms of free radical oxidation of
584 unsaturated lipids. Lipids 30, 277–290.
585 Ratledge, C., 1994. Biodegradation of oils, fats and fatty acids. In: Ratledge, C. (Ed.),
586 Biochemistry of Microbial Degradation. Kluwer Academic Publishers, Dordrecht, pp.
587 89–142.
588 Riebesell U., Schloss I., Smetacek V., 1991. Aggregation of algae released from melting sea
589 ice-implications for seeding and sedimentation. Polar Biology 11, 239–248.
590 Robson, J.N., Rowland, S.J., 1988. Biodegradation of highly branched isoprenoid
591 hydrocarbons: a possible explanation of sedimentary abundance. Organic
592 Geochemistry 13, 691–695.

Rontani, J.-F., Mouzdahir, A., Michotey, V., Bonin P., 2002. Aerobic and anaerobic metabolism of squalene by a new denitrifying *Marinobacter* sp. isolated from marine sediment. Archives of Microbiology 178, 279–287.

Rontani, J.-F., Aubert, C., 2005. Characterization of isomeric allylic diols resulting from chlorophyll phytyl side chain photo- and autoxidation by electron ionization gas chromatography/mass spectrometry. Rapid Communications in Mass Spectrometry 19, 637–646.

Rontani, J.-F., Belt, S.T., Vaultier, F., Brown, T.A., 2011. Visible light-induced photo-oxidation of highly branched isoprenoid (HBI) alkenes: a significant dependence on the number and nature of the double bonds. Organic Geochemistry 42, 812–822.

Rontani, J.-F., Charriere, B., Forest, A., Heussner, S., Vaultier, F., Petit, M., Delsaut, N., Fortier, L., Sempéré, R., 2012. Intense photooxidative degradation of planktonic and bacterial lipids in sinking particles collected with sediment traps across the Canadian Beaufort Shelf (Arctic Ocean). Biogeosciences 9, 4787–4802.

Rontani, J.-F., Bonin, P., Vaultier, F., Guasco, S., Volkman, J.K., 2013a. Anaerobic bacterial degradation of pristenes and phytenes in marine sediments does not lead to pristane and phytane. Organic Geochemistry 58, 43–55.

Rontani, J.-F., Volkman, J.K., Prahl, F.G., Wakeham, S.G., 2013b. Biotic and abiotic degradation of alkenones and implications for $U_{37}^{K'}$ paleoproxy applications: A review. Organic Geochemistry 59, 93–113.

Rontani, J.-F., Belt, S., Vaultier, F., Brown, T., Massé, G., 2014. Autoxidative and photooxidative reactivity of highly branched isoprenoid (HBI) alkenes. Lipids 49, 481–494.

Rontani, J.-F., Belt, S.T., Brown, T.A., Amiraux, R., Gosselin, M., Vaultier, F., Mundy, C.J., 2016. Monitoring abiotic degradation in sinking versus suspended Arctic sea ice algae

during a spring ice melt using specific lipid oxidation tracers. Organic Geochemistry 98, 82–97.

Rontani, J.-F., Galeron, M.-A., Amiraux, R., Artigue, L., Belt, S.T., 2017. Identification of di- and triterpenoid lipid tracers confirms the significant role of autoxidation in the degradation of terrestrial vascular plant material in the Canadian Arctic. Organic Geochemistry 108, 43–50.

Rontani, J.-F., Belt, S.T., Amiraux R., 2018a. Biotic and abiotic degradation of the sea ice diatom biomarker IP_{25} and selected algal sterols in near-surface Arctic sediments. Organic Geochemistry 118, 73–88.

Rontani, J.-F., Smik, L., Belt, S.T., Vaultier, F., Armbrecht, L., Leventer, A., Armand, L.K., 2018b. Abiotic degradation of highly branched isoprenoid alkenes and other lipids in the water column off East Antarctica. Marine Chemistry (Submitted).

Rontani, J.-F., Aubert, C., Belt S.T., 2018c. EIMS Fragmentation and MRM quantification of bacterial metabolites of the sea ice biomarker proxy IP_{25} in Arctic sediments. Rapid Communications in Mass Spectrometry 32, 775–783.

Rowland, S.J., Hird, S.J., Robson, J.N., Venkatesan, M.I., 1990. Hydrogenation behaviour of two highly branched C_{25} dienes from Antarctic marine sediments. Organic Geochemistry 15, 215–218.

Ruan, J., Huang, Y., Shi, X., Liu, Y., Xiao, W., Xu, Y., 2017. Holocene variability in sea surface temperature and sea ice extent in the northern Bering Sea: A multiple biomarker study. Organic Geochemistry 113, 1–9.

Ruiz-Hitzky, E., Casal, B., 1985. Epoxide rearrangements on mineral and silica-alumina surfaces. Journal of Catalysis 92, 291–295.

Rustemov, S.A., Golovieva, L.A., Alieva, R.M., Baskunov, B.P., 1991. New pathway of styrene oxidation by a *Pseudomonas putida* culture. Mikrobiologiya 61, 5–10.

643 Schaich, K.M., 2005. Lipid oxidation: Theoretical aspects. In: Shahidi, F. (Ed.), Bailey's
644 Industrial Oil and Fat Products. John Wiley & Sons, Chichester, pp. 269–355.
645 Seki, H., Ohyama, K., Sawai, S., Mizutani, M., Ohnishi, T., Sudo, H., Akashi, T., Aoki, T.,
646 Saito, K., Muranaka, T., 2008. Licorice β-amyrin 11-oxidase, a cytochrome P450 with
647 a key role in the biosynthesis of the triterpene sweetener glycyrrhizin. Proceedings of
648 the National Academy of Sciences 105, 14204–14209.
649 Sinninghe Damsté, J.S., Schouten, S., Rijpstra, W.I.C., Hopmans, E.C., Peletier, H., Gieskes,
650 W.W.C., Geenevasen, J.A.J., 1999. Structural identification of the C_{25} highly branched
651 isoprenoid pentaene in the marine diatom *Rhizosolenia setigera*. Organic
652 Geochemistry 30, 1581–1583.
653 Sinninghe Damsté, J.S., Muyzer, G., Abbas, B., Rampen, S.W., Massé, G., Allard, W.G.,
654 Belt, S.T., Robert, J.-M., Rowland, S.J., Moldowan, J.M., Barbanti, S.M., Fago, F.J.,
655 Denisevich, P., Dahl, J., Trinidade, L.A.F., Schouten, S., 2004. The rise of the
656 rhizosolenid diatoms. Science 304, 584–587.
657 Soltani, M., Metzger, P., Largeau, C., 2004. Effects of hydrocarbon structure on fatty acid,
658 fatty alcohols and β-hydroxy acid composition in the hydrocarbon-degrading
659 bacterium *Marinobacter hydrocarbonoclasticus*. Lipids 39, 491–505.
660 Stein, R., Fahl, K., Müller, J., 2012. Proxy reconstruction of Arctic Ocean sea ice history:
661 from IRD to IP_{25}. Polarforschung 82, 37–71.
662 Swaving, J., de Bont, A.M., 1998. Microbial transformation of epoxides. Enzyme and
663 Microbial Technology 22, 19–26.
664 Vare, L.L., Massé, G., Gregory, T.R., Smart, C.W., Belt, S.T., 2009. Sea ice variations in the
665 central Canadian Arctic Archipelago during the Holocene. Quaternary Science
666 Reviews 28, 1354–1366.

667 Volkman, J.K., Barrett, S.M., Dunstan, G.A., 1994. C_{25} and C_{30} highly branched isoprenoid
668 alkenes in laboratory cultures of two marine diatoms. Organic Geochemistry 21, 407–
669 414.
670 Xiao, X., Stein, R., Fahl, K., 2013. Biomarker distributions in surface sediments from the
671 Kara and Laptev Seas (Arctic Ocean): Indicators for organic-carbon sources and sea
672 ice coverage. Quaternary Science Reviews 79, 40–52.
673 Zabeti, N., Bonin, P., Volkman, J.K., Jameson, I., Guasco, S., Rontani, J.-F., 2010. Potential
674 alteration of $U_{37}^{K'}$ paleothermometer due to selective degradation of alkenones by
675 marine bacteria isolated from the haptophyte *Emiliania huxleyi*. FEMS Microbiology
676 and Ecology 73, 83–94.

APPENDIX

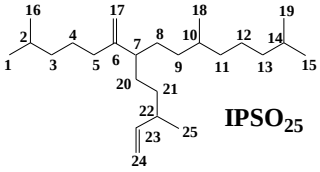

IPSO$_{25}$

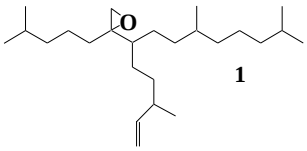

1

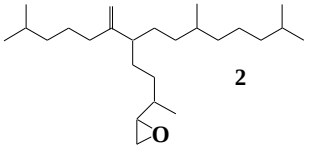

2

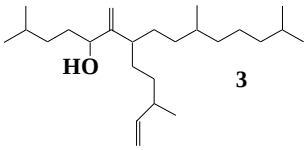

3

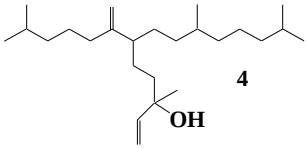

4

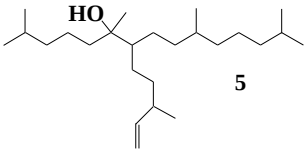

5

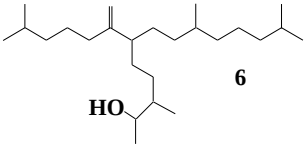

6

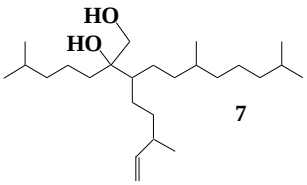

7

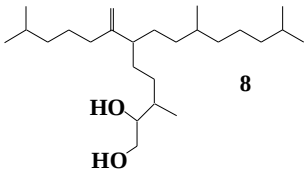

8

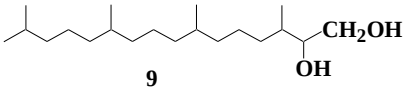

9

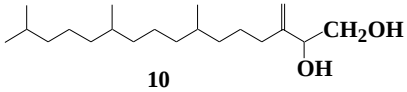

10

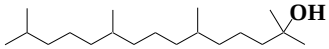

11

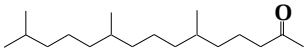

12

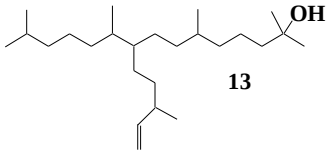

13

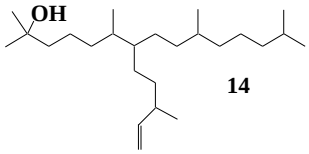

14

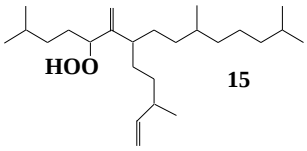

15

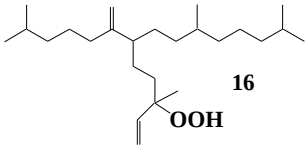

16

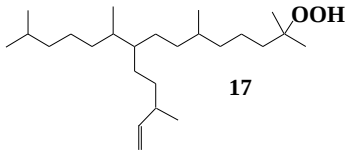

17

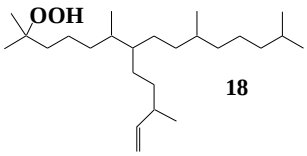

18

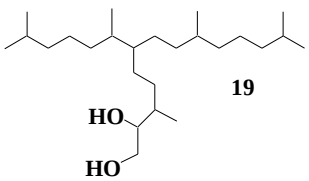

19

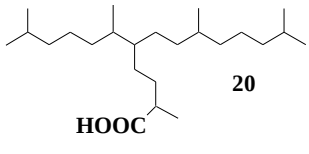

20

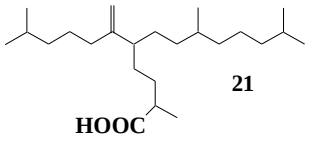

21

678 **Figure captions**

679

680 **Fig. 1**. TOFMS mass spectra of 1,2-epoxy-2-(4-methylpentyl)-3-(3-methylpent-4-enyl)-6,10-
681 dimethylundecane (**1**) (A) and trimethylsilyl derivatives of: 6-methylidene-2,10,14-trimethyl-
682 7-(3-methylpent-4-enyl)-pentadecan-5-ol (**3**) (B), 3,9,13-trimethyl-6-(1-methylidene-5-
683 methylhexyl)-tetradec-1-en-3-ol (**4**) (C) and 10-methylidene-2,6,14-trimethyl-9-(3-
684 methylpent-4-enyl)-pentadecan-2-ol (**13**) or 6-methylidene-2,10,14-trimethyl-7-(3-
685 methylpent-4-enyl)-pentadecan-2-ol (**14**) (D).

686

687 **Fig. 2**. TOFMS mass spectra of trimethylsilyl derivatives of: 2,6,10,14-tetramethyl-7-(3-
688 methylpent-4-enyl)-pentadecan-6-ol (**5**) (A), 3,9,13-trimethyl-6-(1-methylidene-5-
689 methylhexyl)-tetradecan-2-ol (**6**) (B), 2-(4-methylpentyl)-3-(3-methylpent-4-enyl)-6,10-
690 dimethylundecane-1,2-diol (**7**) (C) and 3,9,13-trimethyl-6-(1-methylene-5-methylhexyl)-
691 tetradecane-1,2-diol (**8**) (D) .

692

693 **Fig. 3**. MRM chromatograms (*m*/*z* 365 → 275, *m*/*z* 365 → 149 and *m*/*z* 425 → 135) of
694 silylated standard alcohol **3** (A) and DCM fractions obtained from the Antarctic station BC
695 313 (B) and the 10–11 cm sediment layer of the box core from Barrow Strait (Canadian
696 Arctic) (C).

697

698 **Fig. 4**. MRM chromatograms (*m*/*z* 201 → 111, *m*/*z* 353 → 117, *m*/*z* 353 → 297 and *m*/*z* 423
699 → 367) of silylated standard alcohol **5** (A) and DCM fraction obtained from the 2–3 cm
700 sediment layer of the box core from Barrow Strait (Canadian Arctic) (B).

701

Fig. 5. MRM chromatograms (*m*/*z* 526 → 231 and *m*/*z* 526 → 142) of silylated standard diol **7** (A) and DCM fractions obtained from the 2–3 cm (B) and the 10–11 cm (C) sediment layers of the box core from Barrow Strait (Canadian Arctic).

Fig. 6. Proposed mechanisms for the autoxidation of $IPSO_{25}$ in sediments and subsequent $NaBH_4$-reduction of the resulting hydroperoxides during the treatment.

Fig. 7. Proposed mechanisms for the formation and degradation of epoxides **1** and **2** in sediments.

Fig. 8. Relative percentages of $IPSO_{25}$ and its degradation products in various sediment sections of the box core from Barrow Strait (Canadian Arctic).

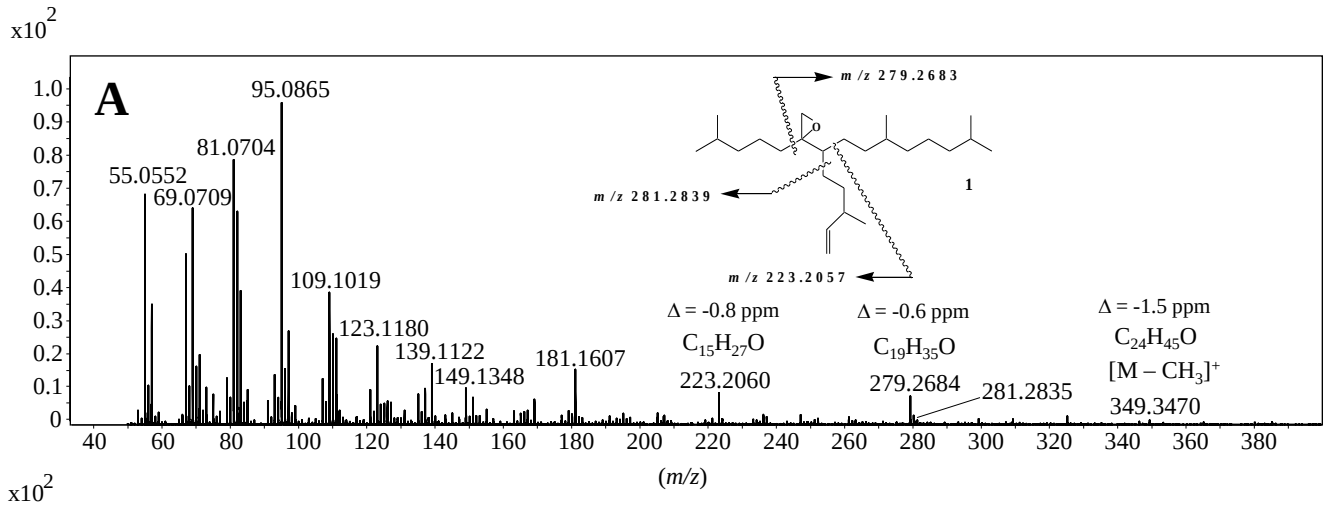
x10^2
A
95.0865
81.0704
55.0552
69.0709
109.1019
123.1180
139.1122
149.1348
181.1607
m /z 279.2683
m /z 281.2839
m /z 223.2057
1
Δ = -0.8 ppm
C15H27O
223.2060
Δ = -0.6 ppm
C19H35O
279.2684
281.2835
Δ = -1.5 ppm
C24H45O
[M – CH3]+
349.3470
(m/z)

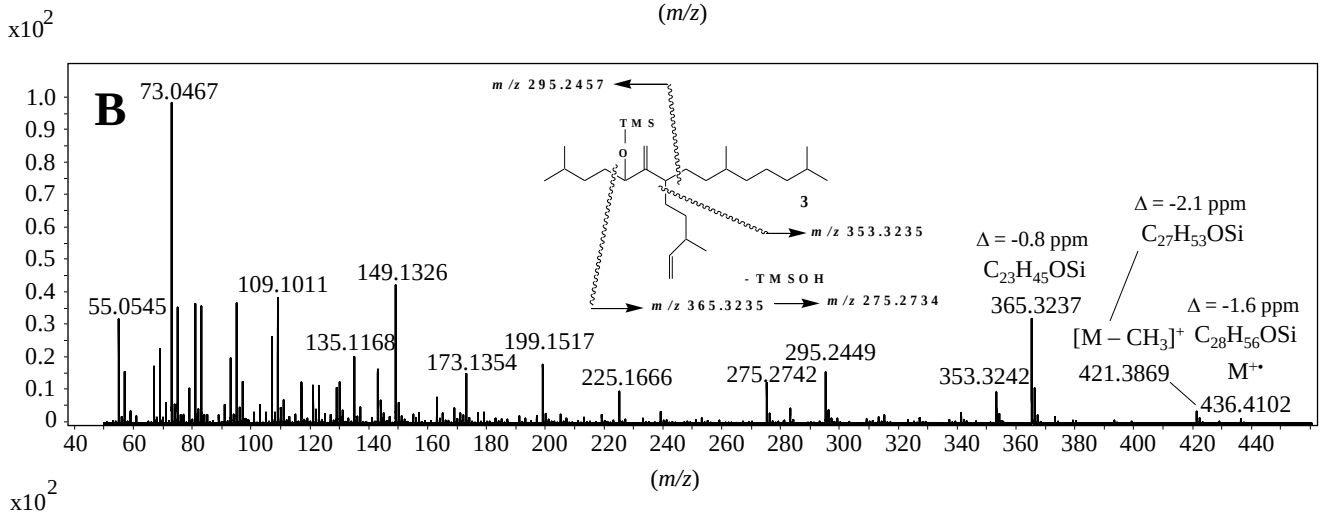
x10^2
B
73.0467
55.0545
109.1011
149.1326
135.1168
173.1354
199.1517
225.1666
275.2742
295.2449
353.3242
365.3237
421.3869
436.4102
m /z 295.2457
TMS
3
m /z 353.3235
- TMSOH
m /z 365.3235
m /z 275.2734
Δ = -2.1 ppm
C27H53OSi
Δ = -0.8 ppm
C23H45OSi
[M – CH3]+
Δ = -1.6 ppm
C28H56OSi
M+•
(m/z)

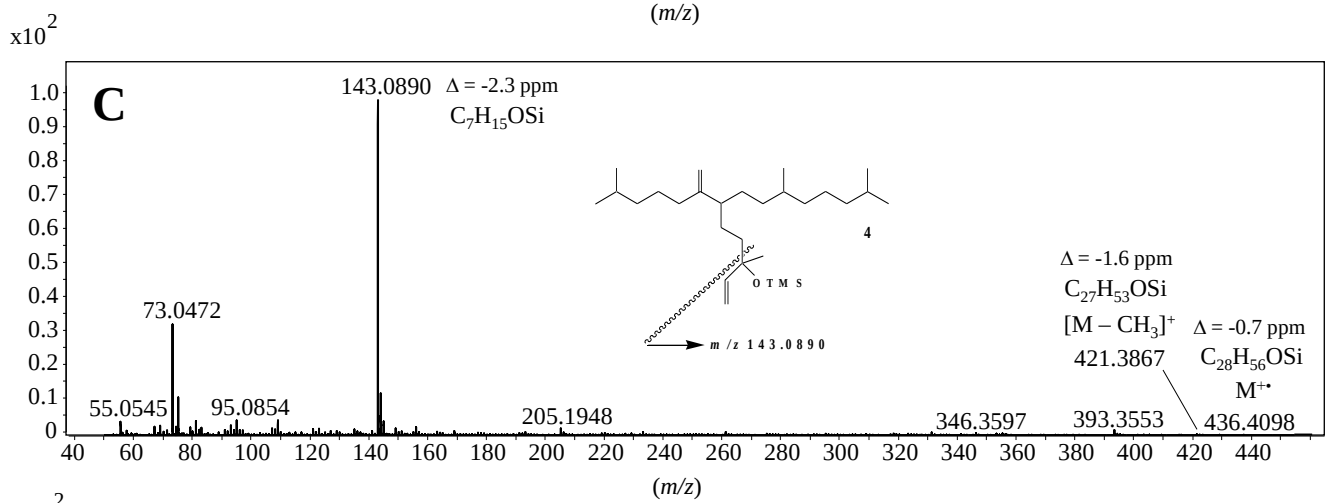
x10^2
C
143.0890
Δ = -2.3 ppm
C7H15OSi
73.0472
55.0545
95.0854
205.1948
346.3597
393.3553
436.4098
4
OTMS
m /z 143.0890
Δ = -1.6 ppm
C27H53OSi
[M – CH3]+
421.3867
Δ = -0.7 ppm
C28H56OSi
M+•
(m/z)

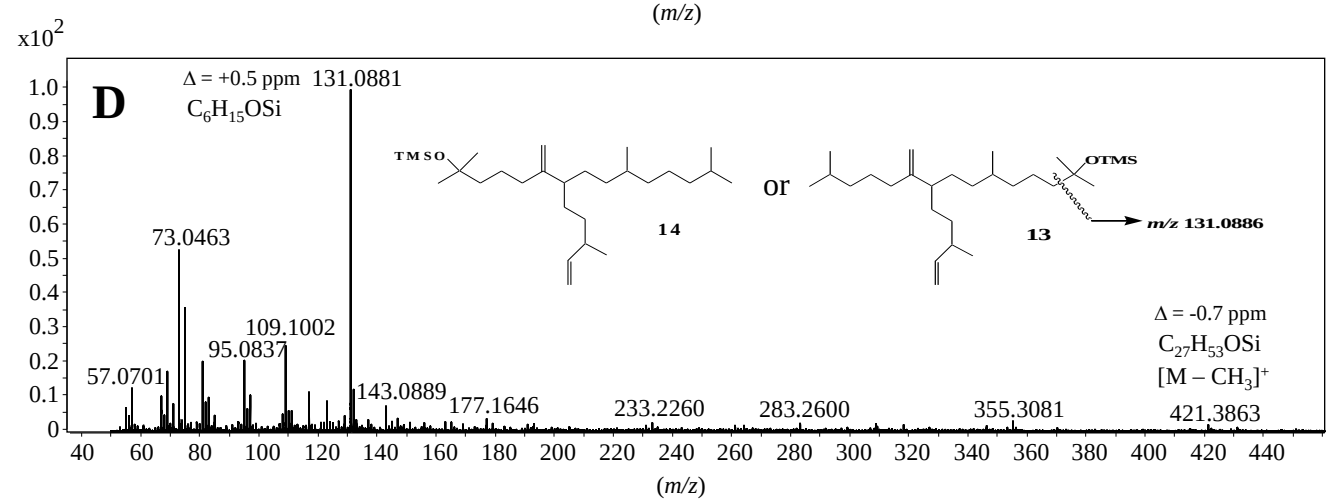
x10^2
D
Δ = +0.5 ppm
C6H15OSi
131.0881
73.0463
109.1002
95.0837
57.0701
143.0889
177.1646
233.2260
283.2600
355.3081
421.3863
TMSO
14
or
OTMS
13
m/z 131.0886
Δ = -0.7 ppm
C27H53OSi
[M – CH3]+
(m/z)

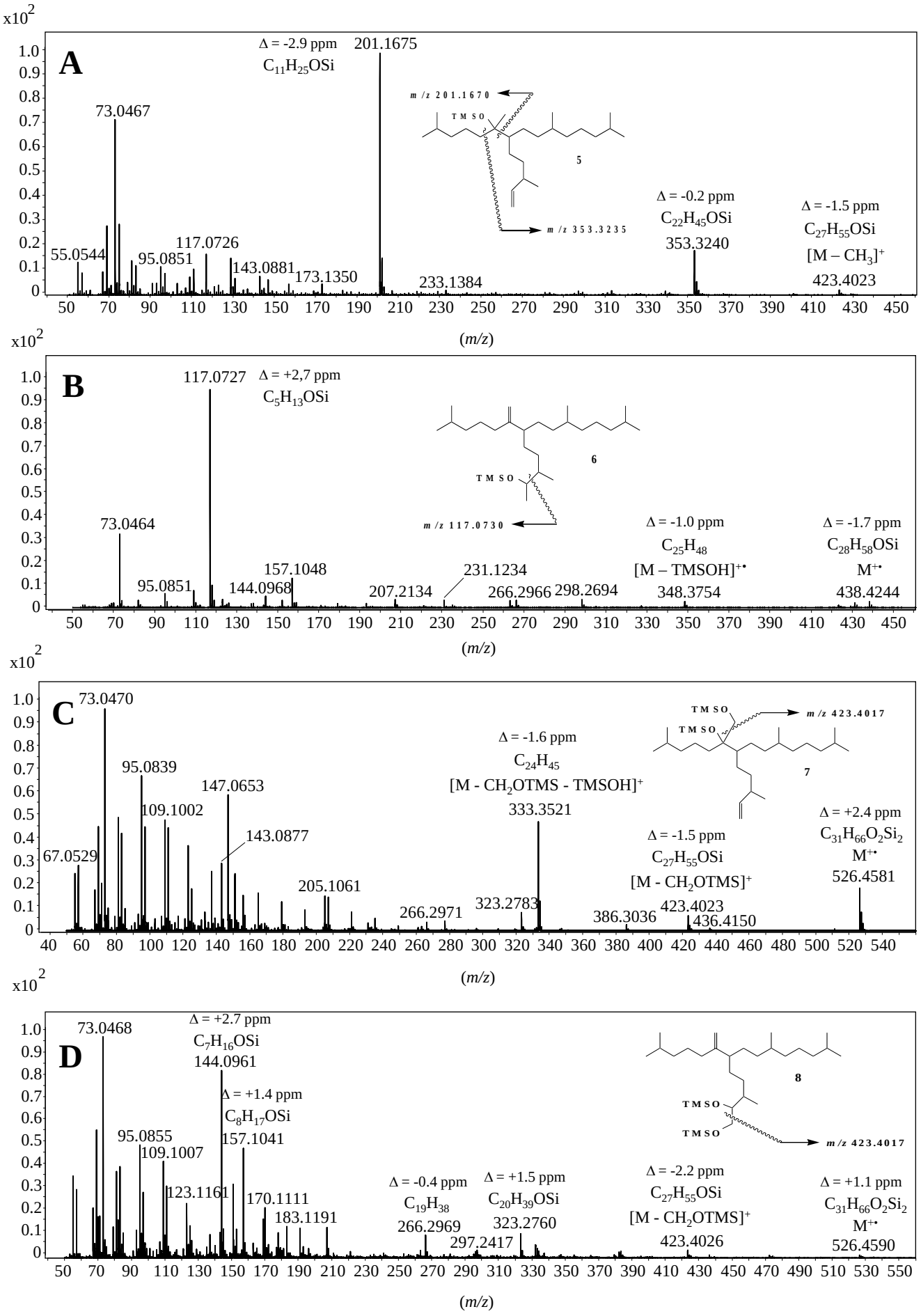
x10^2
A
Δ = -2.9 ppm
C11H25OSi
201.1675
73.0467
117.0726
55.0544
95.0851
143.0881
173.1350
233.1384
m/z 201.1670
TMSO
5
m/z 353.3235
Δ = -0.2 ppm
C22H45OSi
353.3240
Δ = -1.5 ppm
C27H55OSi
[M – CH3]+
423.4023
(m/z)
x10^2
B
117.0727
Δ = +2,7 ppm
C5H13OSi
6
TMSO
m/z 117.0730
73.0464
157.1048
95.0851
144.0968
207.2134
231.1234
266.2966
298.2694
Δ = -1.0 ppm
C25H48
[M – TMSOH]+•
348.3754
Δ = -1.7 ppm
C28H58OSi
M+•
438.4244
(m/z)
x10^2
C
73.0470
95.0839
147.0653
109.1002
143.0877
67.0529
205.1061
266.2971
323.2783
386.3036
423.4023
436.4150
Δ = -1.6 ppm
C24H45
[M - CH2OTMS - TMSOH]+
333.3521
TMSO
TMSO
m/z 423.4017
7
Δ = -1.5 ppm
C27H55OSi
[M - CH2OTMS]+
Δ = +2.4 ppm
C31H66O2Si2
M+•
526.4581
(m/z)
x10^2
D
73.0468
Δ = +2.7 ppm
C7H16OSi
144.0961
Δ = +1.4 ppm
C8H17OSi
157.1041
95.0855
109.1007
123.1161
170.1111
183.1191
Δ = -0.4 ppm
C19H38
266.2969
Δ = +1.5 ppm
C20H39OSi
323.2760
297.2417
8
TMSO
TMSO
m/z 423.4017
Δ = -2.2 ppm
C27H55OSi
[M - CH2OTMS]+
423.4026
Δ = +1.1 ppm
C31H66O2Si2
M+•
526.4590
(m/z)

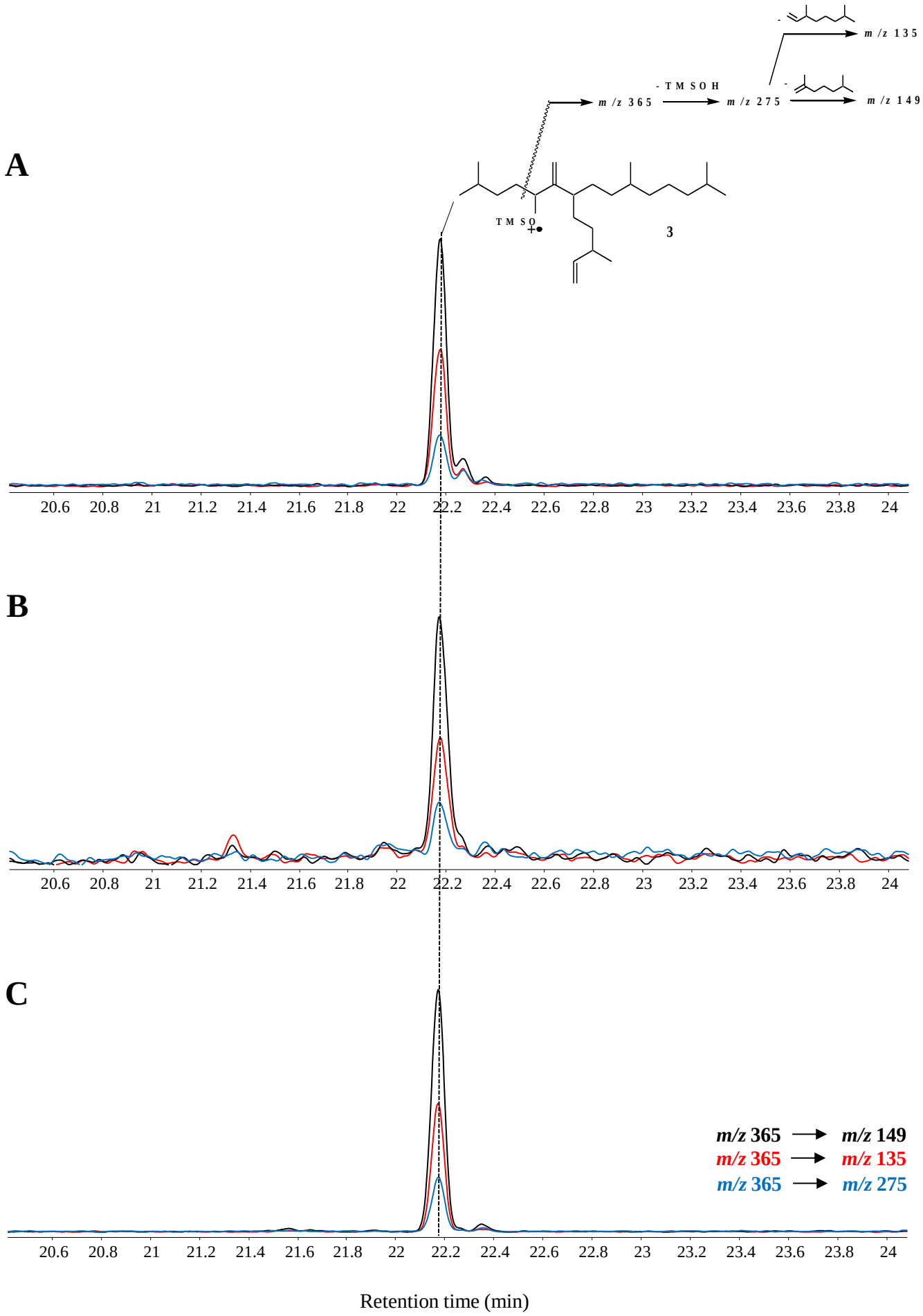
A
B
C
- TMSOH
m /z 365
m /z 275
m /z 149
m /z 135
TMSO
3
m/z 365 → m/z 149
m/z 365 → m/z 135
m/z 365 → m/z 275
20.6 20.8 21 21.2 21.4 21.6 21.8 22 22.2 22.4 22.6 22.8 23 23.2 23.4 23.6 23.8 24
Retention time (min)

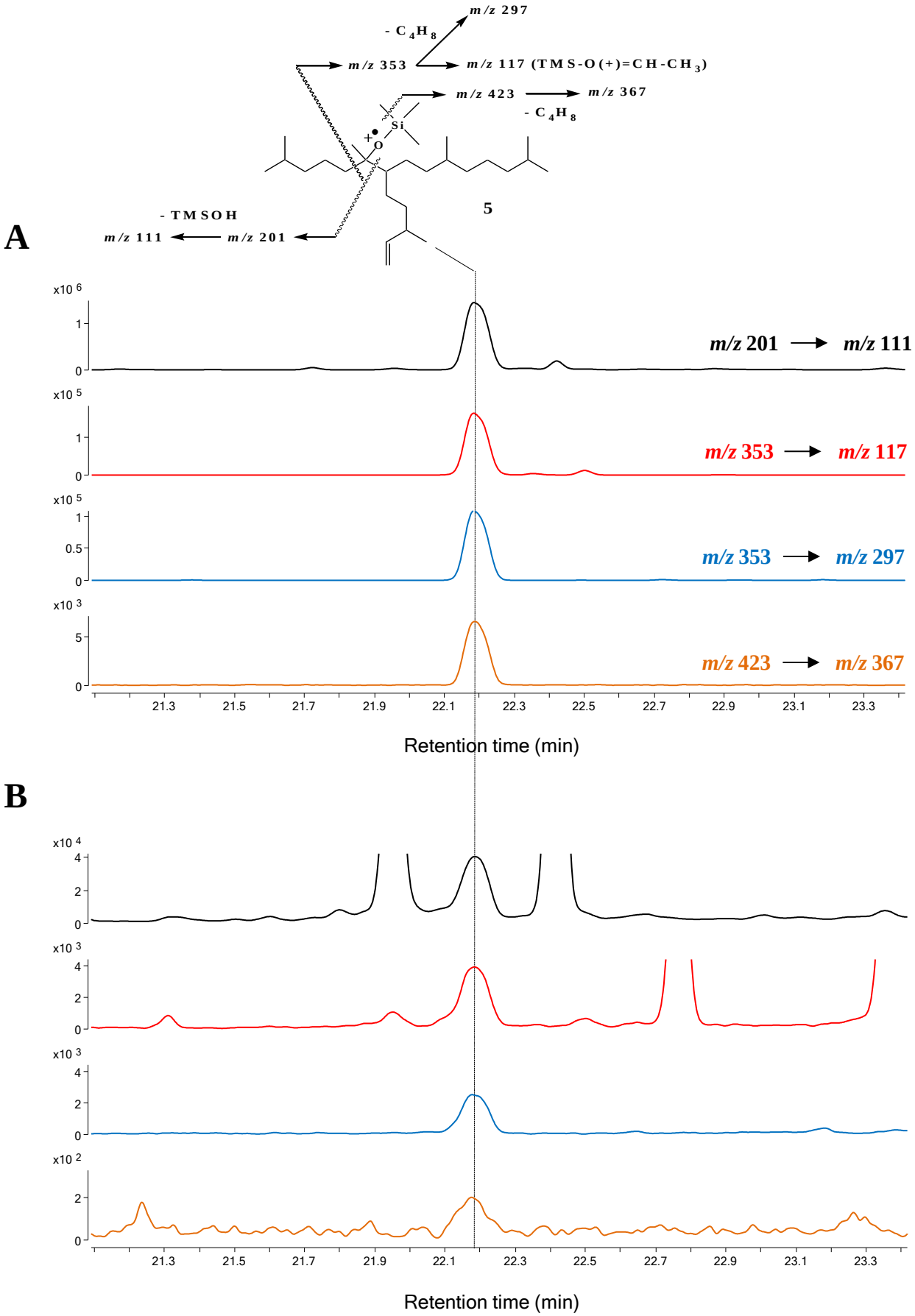
m/z 297
- C4H8
m/z 353
m/z 117 (TMS-O(+)=CH-CH3)
m/z 423
m/z 367
- C4H8
Si
O
5
- TMSOH
m/z 111
m/z 201
A
x10 6
m/z 201 → m/z 111
x10 5
m/z 353 → m/z 117
x10 5
m/z 353 → m/z 297
x10 3
m/z 423 → m/z 367
21.3
21.5
21.7
21.9
22.1
22.3
22.5
22.7
22.9
23.1
23.3
Retention time (min)
B
x10 4
x10 3
x10 3
x10 2
Retention time (min)

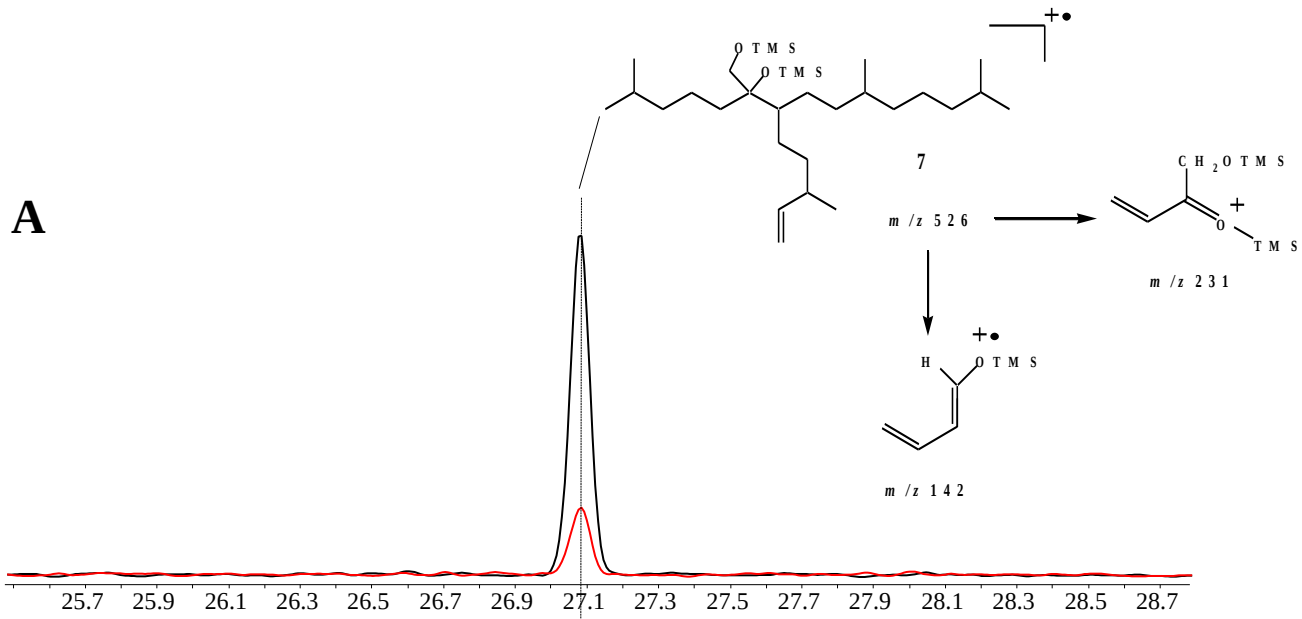
A
OTMS
OTMS
7
m/z 526
CH2OTMS
O
TMS
m/z 231
H
OTMS
m/z 142
25.7 25.9 26.1 26.3 26.5 26.7 26.9 27.1 27.3 27.5 27.7 27.9 28.1 28.3 28.5 28.7
Retention time (min)

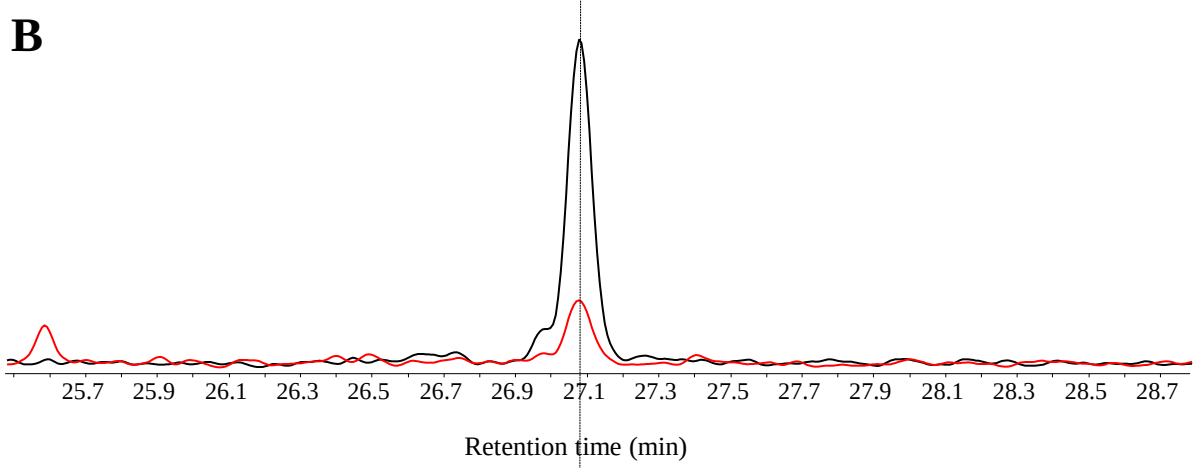
B
25.7 25.9 26.1 26.3 26.5 26.7 26.9 27.1 27.3 27.5 27.7 27.9 28.1 28.3 28.5 28.7
Retention time (min)

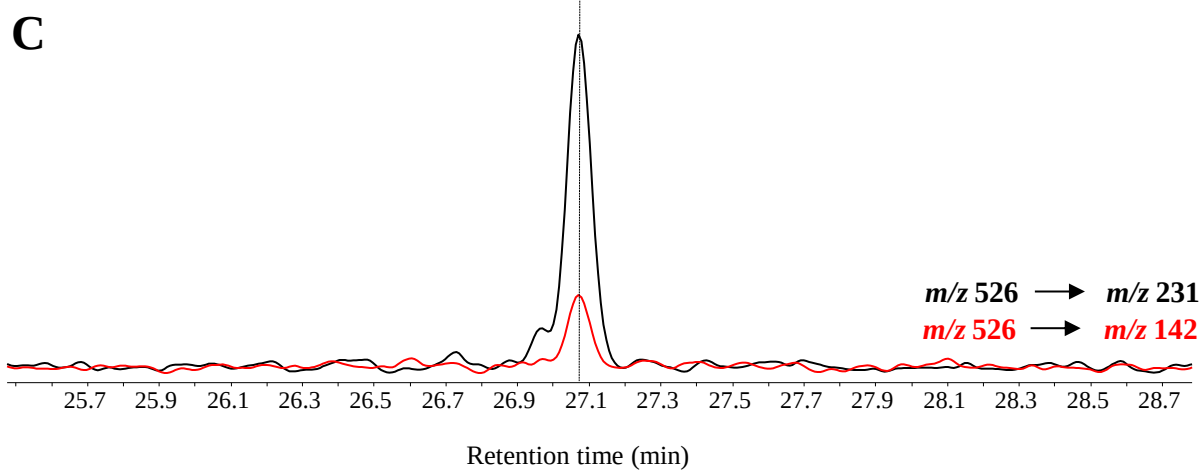
C
m/z 526 → m/z 231
m/z 526 → m/z 142
25.7 25.9 26.1 26.3 26.5 26.7 26.9 27.1 27.3 27.5 27.7 27.9 28.1 28.3 28.5 28.7
Retention time (min)

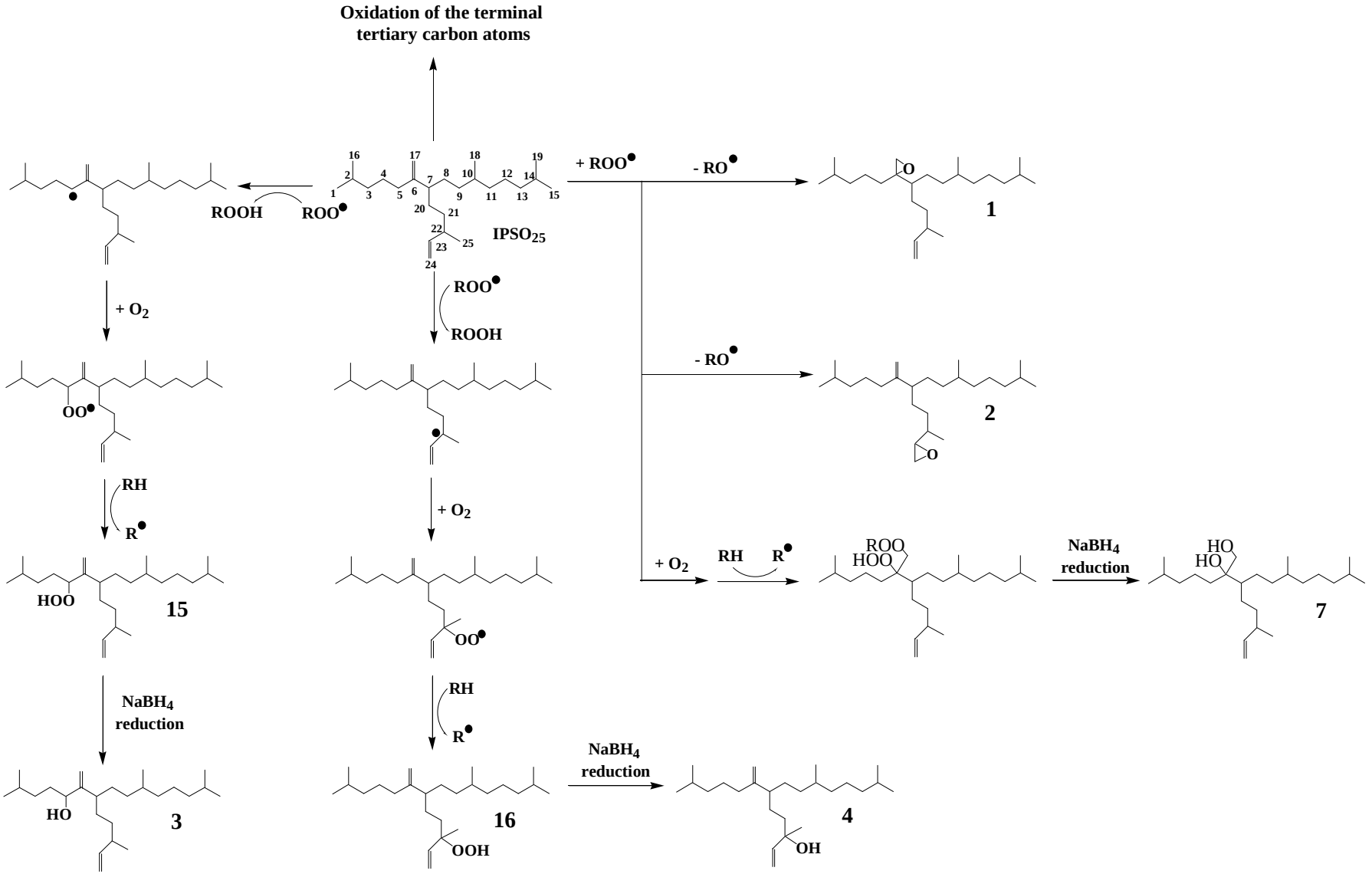
Oxidation of the terminal tertiary carbon atoms
ROOH
ROO●
IPSO25
+ ROO●
- RO●
1
+ O2
ROO●
ROOH
- RO●
2
OO●
RH
R●
+ O2
+ O2
RH
R●
ROO
HOO
NaBH4 reduction
7
HOO
15
OO●
NaBH4 reduction
RH
R●
HO
3
16
OOH
NaBH4 reduction
4
OH

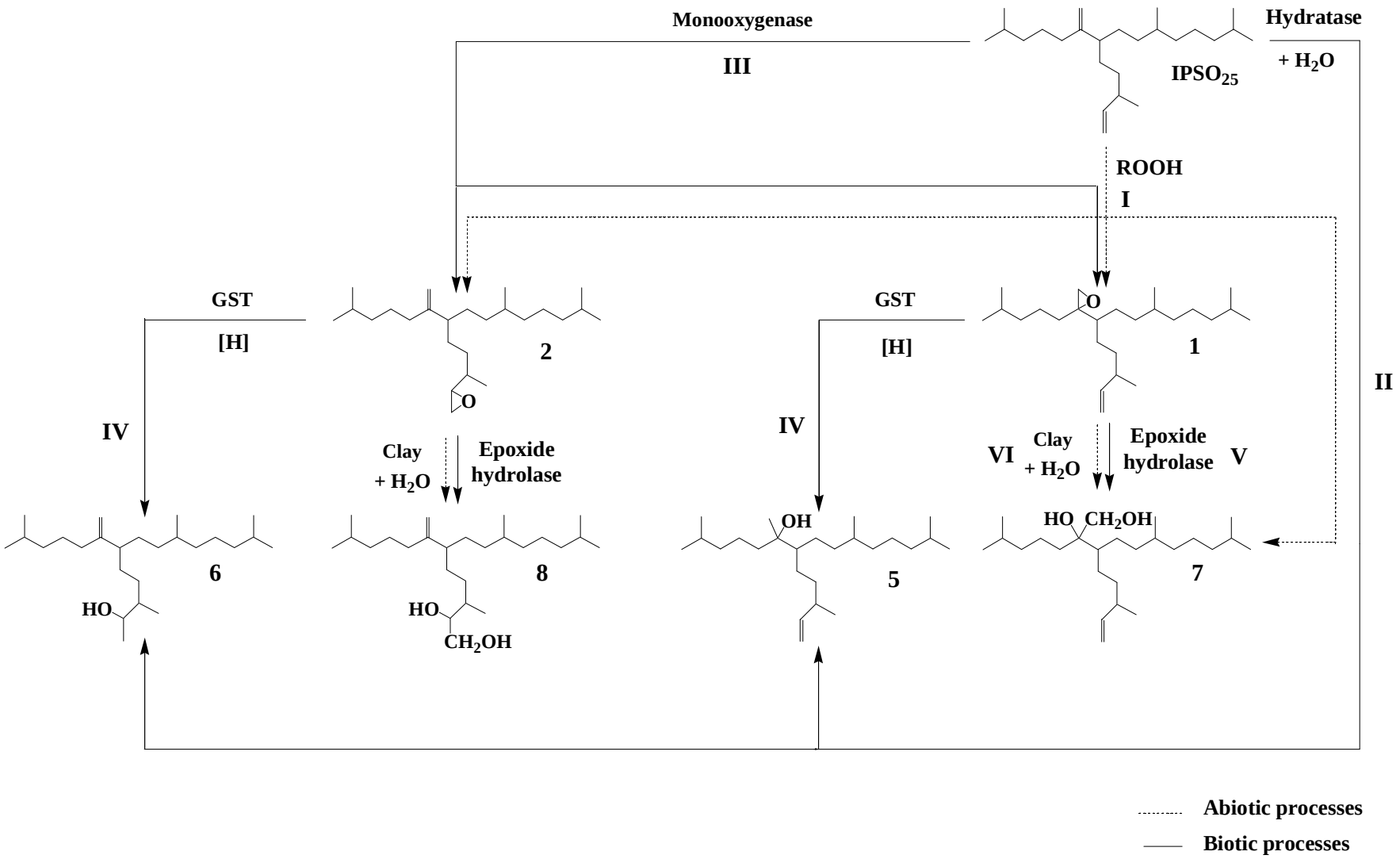
Monooxygenase
III
Hydratase
+ H2O
IPSO25
ROOH
I
II
GST
[H]
IV
2
O
Clay
+ H2O
Epoxide
hydrolase
6
HO
8
HO
CH2OH
GST
[H]
IV
OH
5
O
1
VI
Clay
+ H2O
Epoxide
hydrolase
V
HO CH2OH
7
Abiotic processes
Biotic processes

Relative percentage of $IPSO_{25}$ and its degradation products

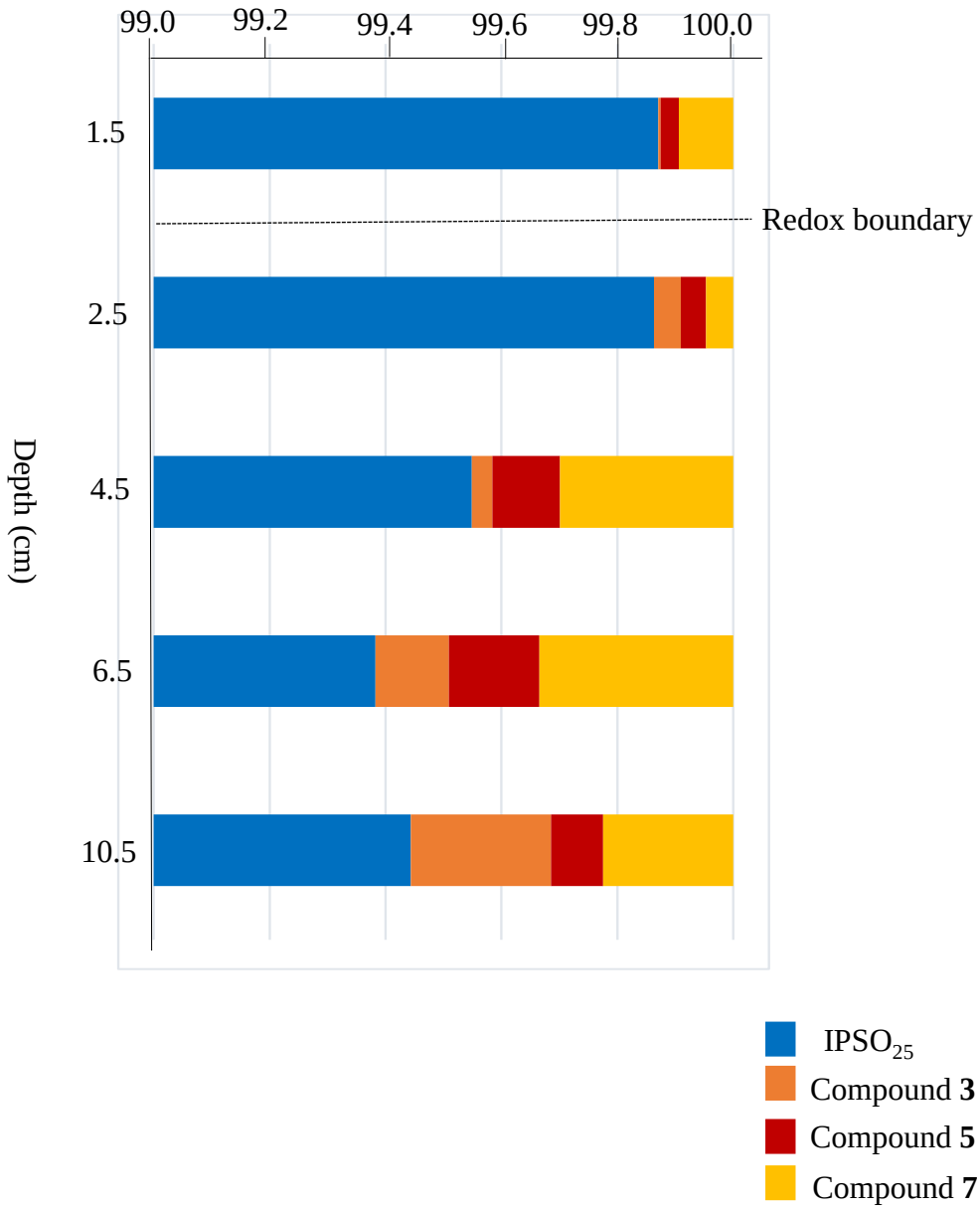

Table 1

Concentrations of $IPSO_{25}$ and its degradation products in Antarctic surface sediments (note the difference in units between $IPSO_{25}$ and its oxidation products).

Station	$IPSO_{25}$ (ng g^{-1})	Compound **3** (pg g^{-1})	Compound **5** (pg g^{-1})
BC 313	1201.0	101.3 (0.01)[b]	77.8 (0.01)[b]
BC 316	396.0	569.2 (0.14)	38.1 (0.01)
BC 516	49.0	50.0 (0.10)	-
BC 566	42.0	230.3 (0.55)	231.7 (0.55)
BC 571	14.0	44.4 (0.32)	37.0 (0.26)
BC 615	93.0	-[a]	33.4 (0.04)
BC 628	29.0	54.5 (0.19)	25.4 (0.01)

[a] Not detected
[b] Percentage relative to the residual parent compound.

Table 2

Concentrations of $IPSO_{25}$ and its degradation products in sediments from the Arctic station 4 (Barrow Strait) (note the difference in units between $IPSO_{25}$ and its oxidation products).

Depth (cm)	$IPSO_{25}$ ($\mu g\ g^{-1}$)	Compound **3** ($ng\ g^{-1}$)	Compound **5** ($ng\ g^{-1}$)	Compound **7** ($ng\ g^{-1}$)
1–2	2.5	0.1	0.8	2.4
2–3	3.2	1.5	1.4	1.5
4–5	2.0	0.7	2.3	5.9
6–7	1.7	2.2	2.7	5.8
8–9	1.6	0.2	0.1	0.6
10–11	1.8	4.3	1.6	4.0